Chapter 3

Electrical Properties of Epitaxial Ferroelectric Heterostructures

Andra Georgia Boni, Cristina Florentina Chirila, Raluca Negrea, Corneliu Ghica, Iuliana Pasuk, Ioana Pintilie and Lucian Pintilie

Additional information is available at the end of the chapter

http://dx.doi.org/10.5772/intechopen.70133

Abstract

In the context of miniaturization of devices, ferroelectric materials are used as multifunctional materials for their well-known intrinsic properties, especially for the switching of polarization in an applied electric field. The high-quality epitaxial thin film structures are used for the possibility to study different effects as low dimensions, interface, strain and strain gradients on ferroelectric materials and other electric characteristics, also representing a possibility to obtain new phenomena and properties that can be used for development of new devices with different functionalities. This chapter is a summary of the ferroelectric and dielectric behaviour of epitaxial thin films of $Pb(Zr,Ti)O_3$ (PZT) and $BaTiO_3$ (BTO) obtained by pulsed laser deposition and the correlation with structural quality of the layers and with different electrostatic conditions induced either by electrodes or by the different interlayers. For this purpose in the first part, studies regarding the influence of the substrates and of different top electrodes are performed for $Pb(Zr,Ti)O_3$ (PZT) 52/48. In the second part, we focused on artificial multiferroic structures from alternating layers of PZT 20/80 or $BaTiO_3$ (BTO) as ferroelectric phase and $CoFe_2O_4$ (CFO) as magnetic material. We found that interface configuration and strain engineering could control ferroelectric hysteresis, the capacitance or the leakage current magnitude.

Keywords: ferroelectric thin films, electrical properties, multilayered structures, electrostatic boundary conditions, interfaces

1. Introduction

Ferroelectrics are multifunctional materials possessing special properties derived from the presence of the spontaneous polarization in the absence of an applied electric field. Ferroelectricity is electrical analogue of ferromagnetism, the distinguishing property of ferroelectricity being the possibility of reversing the spontaneous polarization when an external electric field is applied in the opposite direction. As a consequence, the polarization describes a hysteresis loop as magnetization does in ferromagnetic materials. Ferroelectric materials also possess piezoelectric and pyroelectric properties which are used in many electronic applications, such as tunable capacitors, ferroelectric nonvolatile memories, ultrasound sensors or generators and infrared sensors [1–4]. Another interesting topic is related to multiferroic materials—single phase or heterostructures—which possess more than one order parameter (usually magnetic and ferroelectric ordering) and which can lead to new applications if there is a coupling between the order parameters [5–9].

For many applications, the ferroelectrics are used either as bulk ceramics/single crystals or as thin films with different structural qualities, from polycrystalline to epitaxial. The necessary electrical properties for different applications of ferroelectric materials are strongly influenced by the structural quality. For instance, the existence of the grains and grain boundaries in nanostructured thin films/polycrystalline thin films can induce modification on the magnitude of polarization, dielectric constant and so forth. As for the standard semiconductors, the studies of intrinsic electrical properties should be performed on high-quality single-crystal samples. One method to obtain such samples is to deposit thin films of epitaxial quality. The obtaining of epitaxy for ferroelectric materials often involves the deposition of the ferroelectric thin films on single-crystal substrates, with different buffer or electrode layers, resulting in a heteroepitaxial growth of the film. Therefore, the use of materials with different values for the lattice parameters can generate mechanical tensions/deformations and strain in the lattice of the ferroelectric film [10–13].

It is known that, by changing the pressure on ferroelectric bulk ceramics or single crystals, the transition temperature, piezoelectric and dielectric constants can be modified. In the case of thin films, applying significant hydrostatic pressure to induce modification of ferroelectric properties leads to physical cracks of the samples. Thus, the epitaxy offers the possibility to induce strain and strain-polarization coupling for the enhancement of ferroelectric properties. Examples of the influence of the strain in epitaxial heterostructures are enhancement of polarization in $BaTiO_3$ (BTO) [14–16], the shift of the transition temperature for $PbTiO_3$ and $BaTiO_3$ films towards higher values [17], room temperature-induced ferroelectricity in $SrTiO_3$ thin films [14–16] and in un-doped HfO_2 layers [18] or in artificial superlattices [19] formed from non-ferroelectric materials, etc. These phenomena are specific for fully coherent thin films with low density of dislocations. Nevertheless, by growing the thickness of the deposited ferroelectric layer, many dislocations and other defects appear in order to minimize the free energy of the systems. Different lattice relaxation processes could generate strain gradients in the films, which could imply a flexoelectric field. The effects of these supplementary fields lead to different behaviours in polarization switching, shift of the hysteresis loop along

voltage axis, modification of remnant polarization and occurrence of diode-like current characteristics with dependence on polarization direction [20–22].

As complex equivalent circuits are used for many applications involving ferroelectric materials, it ensures that good knowledge of the electric properties of these materials is a very important topic besides the deposition method and the structural quality. The ferroelectric materials/thin films should be integrated in a capacitor-like structure for the study of the electrical properties. Therefore, a common way to build such a structure is to deposit a continuous conductor thin film as bottom electrode, on which ferroelectric thin film is further deposited. On top of this structure, the top electrode is deposited using a shadow mask, which delimitates the active area of the capacitor. The specific measurements can be realized by connecting the measurement circuit on the upper and bottom electrodes.

The most used characterization techniques for investigation of ferroelectric properties are hysteresis loops of polarization versus the applied electric field, small signal capacitance measurements (as dependence of capacitance on voltage, frequency or temperature) and leakage current. These characteristics offer information about the ferroelectric character of the structure (e.g. the measurement of a rectangular hysteresis loop or a butterfly shape of the capacitance-voltage characteristics) or the values for different parameters of interest (dielectric constant, coercive field, magnitude of polarization and transition temperature).

One of the most studied classes of ferroelectric materials is oxide ferroelectrics, especially the subclass of the materials with perovskite structure. $BaTiO_3$ and $Pb(Zr,Ti)O_3$ (PZT) are the most investigated materials from this category from the point of view of applications. In this chapter, we will present the electrical and ferroelectric properties for this type of epitaxial ferroelectric thin films, obtained by pulsed laser deposition (PLD), and their dependence on the type of the substrate used for deposition or on the material used for the top electrode. Further on, we will show that, by constructing artificially layered structures from thin films of ferroelectric materials and materials having different electric/dielectric properties, the ferroelectric/electric properties can be modified and engineered to obtain enhanced or even new properties. For example, due to either electromechanical or electrostatic interactions, a tuning of capacitance, switching behaviour or leakage current magnitude can be realized.

2. Epitaxy

The term epitaxy refers to a film growth on a substrate with crystallographic structure close to that of the deposited layer. Epitaxial growth is one of the most important techniques in the present microelectronic industry, allowing a better correlation between structure and the macroscopic properties of thin films. Important problems can be studied in this way, related to physics of surfaces, interfaces and strain engineering. There are a wide variety of growth techniques that can be used to obtain epitaxial thin films including sputtering, metal-organic chemical vapour deposition, pulsed laser deposition, molecular beam epitaxy, physical vapour deposition, etc. In this chapter, we will discuss the heteroepitaxial growth, by pulsed

laser deposition, of oxide thin films with ferroelectric/multiferroic properties. There are three known growth modes: (1) Frank-Van der Merwe, layer-by-layer growth; (2) Volmer-Weber, island growth and (3) Stranski-Krastanov, a combination of layer-by-layer and island growth. Thermodynamic approach was used in order to explain these growth modes in close to equilibrium conditions [23]. The balance between free energies from the film surface (γ_F), the substrate surface (γ_S) and the interface between them (γ_I) is the key factor that determines the thin film morphology in this approach. Frank-Van der Merwe growth mode is characterized by the fact that the deposited atoms or molecules are more strongly bonded to the substrate than in between them, thus forming a continuous layer on the substrate. In the case of the Volmer-Weber growth mode, the atoms and molecules are more strongly bonded in between them, forming island on the substrate, thus the wetting of the substrate is poor. Stranski-Krastanov mode is characterized by the fact that, at the beginning of the growth, the atoms and molecules form complete monolayers on the substrate (layer-by-layer growth, usually 1–5 monolayers), and then islands start to develop (growth mode changes to island formation). The transition from monolayers to islands is caused by increased tensions (strain) from increasing the layer thickness. Experimentally, the growing of thin films is not an equilibrium process; therefore kinetic effects have to be taken into account, leading to the occurrence of different growth modes. The above-mentioned growth modes and their schematic representations are shown in **Figure 1**.

A preliminary substrate preparation has to be achieved in order to obtain heteroepitaxial thin films on single-crystal $SrTiO_3$ (STO) substrates. The substrate preparation consists in transforming an optically polished surface into a step-and-terrace surface that is well ordered even on an atomic scale. For this purpose, the $SrTiO_3$ substrates are etched in NH_4-HF solution to remove Sr residue and to obtain a purely Ti-terminated surface and to get a high-quality step-and-terrace structure on the surface. All step edges should have equal height (single unit cell ~ 0.4 nm), and the steps should be approximately parallel and equidistant. This can be obtained after an annealing process, at elevated temperatures, of the etched substrates. The substrate transformation after each processing step is investigated by atomic force microscopy, and the results are presented in **Figure 2**.

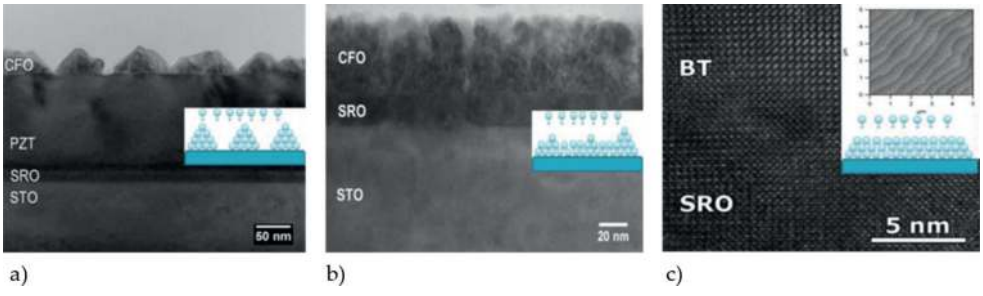

Figure 1. Growth modes for epitaxial thin films: (a) Frank-Van der Merwe, (b) Stranski-Krastanov and (c) Volmer-Weber.

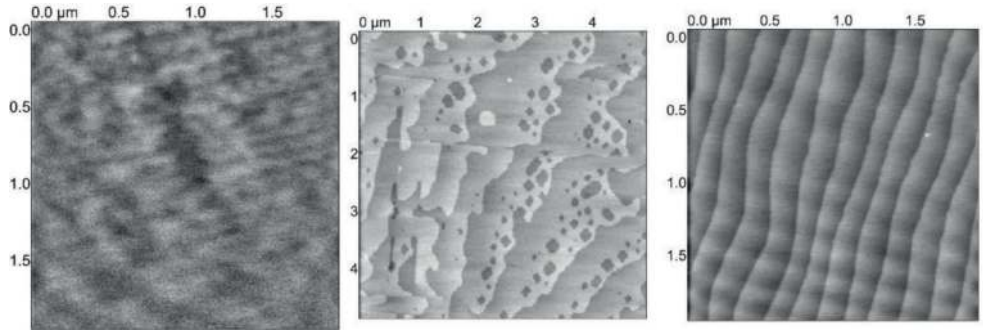

Figure 2. Atomic force microscopy images obtained on STO substrate after each processing step: upper image, fresh substrate; middle image, substrate after etching; and lower image, substrate after thermal annealing.

3. Growth method

Pulsed laser deposition, as the name suggests, is a technique, which uses pulses of laser radiation to remove material from the surface of a solid target. The technique involves complex physical aspects as follows:

1. Interaction between the laser radiation and the target material—high temperature is achieved over a small area (the area of the laser spot) due to the high power of the laser beam in the short period of the laser pulse; this leads to a number of processes occurring at the target surface, such as material decomposition, ionization and evaporation. One has to mention that the target has the same chemical composition as the film intended to be deposited on the substrate.
2. Transfer of the ablated material: the evaporated material from the step 1 forms a plasma plume over the substrate on which the film has to be deposited.
3. Deposition of the ablated material on the substrate—this step consists in the adsorption/chemisorption of the ablated material on the surface of the substrate. One has to mention that the substrate is, usually, heated.
4. Nucleation and growth of the film on the surface of the substrate—the main condition for this process to occur is represented by the balance between free energies from the film surface, the substrate surface and the interface between them.

Each step involved in the pulsed laser deposition process is crucial for obtaining the hetero-epitaxial growth of the thin films.

3.1. Experimental setup

The experimental setup is designed for the deposition of thin films and multilayers from oxide materials and consists of an excimer laser source (KrF, λ = 248 nm) with a pulse duration of

20 ns; a target carrousel with four targets of 2″ diameter, allowing permanent rotation of each target; a substrate holder with controlled motion on five axes and possibility to heat the substrate up to 1000°C; a deposition chamber allowing base vacuum down to 10^{-7} mbar; and high-pressure reflection high-energy electron diffraction (RHEED) system for in situ characterization. The entire system is controlled by PC and is presented in **Figure 3**.

The energy density of the laser pulse (fluence) can reach 5 J/cm^2, and the repetition rate is in the 1–10 Hz range. The laser beam is delivered on the target surface at an angle 45° to the normal. The pressure inside the chamber can be varied during the deposition by changing the flow rate of deposition gas (O_2 or Ar) using mass flow controllers. The substrate temperature is controlled with a proportional–integral–derivative controller (PID controller) temperature controller from room temperature (RT) up to 1000°C. The distance between target and substrate can be adjusted from 40 to 80 mm. All these parameters have to be optimized for each material in order to get the desired heteroepitaxial thin films.

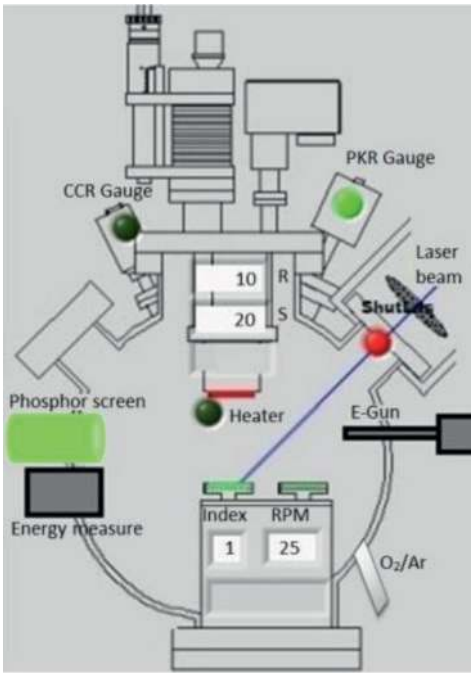

Figure 3. Schematic view of the pulsed laser deposition system.

4. Epitaxial ferroelectric thin films: structural and electrical properties

One representative and widely studied material of the class of perovskite ferroelectrics is lead titanate-zirconate Pb(Zr,Ti)O_3 (PZT). Its phase diagram is quite complex, and its structural,

ferroelectric, pyroelectric and piezoelectric properties depend on temperature, strain and Zr/Ti ratio. Around Zr/Ti ratio of 52/48 this material presents a morphotropic phase boundary, and this composition is often preferred due to enhanced dielectric constant and/or piezoelectric coefficient [24–27].

In the last years, great efforts have been dedicated to the epitaxial growth of ferroelectric thin films with the purpose of obtaining enhanced properties compared to that of the polycrystalline ones. There are many reports on obtaining high-quality epitaxial PZT thin films, deposited by various methods on single-crystal substrates with perovskite structures such as $SrTiO_3$ (STO), but there is an increased need to obtain the same material performances on substrates (Si) allowing rapid integration of ferroelectric materials in the existing complementary metal–oxide–semiconductor (C-MOS) technology. First attempts to deposit PZT layers on Si were realized in the context of constructing metal-ferroelectric-semiconductor field-effect transistors, and it was found out that silicates or other parasitic phases are formed at the PZT-Si interface [28]. To overcome these problems, insulating buffer layers were used as barriers to avoid diffusion of Pb atoms towards Si interface, but this method leads to high depolarization fields. As a consequence, the polarization magnitude decreases, and the retention properties are deteriorated [29–32].

In this context, our first results presented in this section consist in evidencing epitaxial deposition by PLD of PZT on Si (001) using as interlayer a MBE-deposited thin film of STO which acts as a barrier for Pb diffusion and as a template for the growth of the subsequent layers. A 20 nm film of $SrRuO_3$ (SRO) has been deposited by PLD to serve as bottom electrode, and then the PZT film was grown. Even if an epitaxial structure is obtained using this configuration of deposited layers, many structural and electrical differences are observed compared to the same ferroelectric capacitor structure deposited on single-crystal STO substrate [33].

XRD $2\theta-\omega$ diagrams are presented in **Figure 4** for both types of samples, PZT/SRO/STO/Si and PZT/SRO/STO, showing only (00l) (l = 1,2,3,4) maximas for PZT, SRO and STO layers, indicating an out-of-plane-oriented pseudocubic structure for both cases. Around SRO and STO peaks, the layered fringes evidenced in the inset figures are specific for epitaxial thin films and indicate very smooth and parallel interfaces. The PZT out-of-plane lattice parameter is calculated from this data, and a significantly larger value is obtained in the case of the single-crystal STO substrate (c_{PZT} = 4.113 Å) compared to the case of Si substrate with STO buffer layer (c_{PZT} = 4.055 Å). In addition, the rocking curves recorded around 002 lines suggest a better alignment of the crystal planes for PZT films deposited on STO substrate, with a full width at half maximum of 0.2°, compared to 0.6° in the case of the PZT films deposited on STO-buffered Si substrate. Phi scans were performed on tilted crystalline planes to evidence the cube-on-cube growing relation between PZT, SRO and STO and to determine the (001) orientation relation between the planes of the Si substrate and those of the oxide layers (see **Figure 4**). The epitaxial growth is confirmed by obtaining the four peaks, related to the four-fold rotation axis of the pseudocubic symmetry. The in-plane orientation relations are such that PZT[100]//SRO[100]//STO[100]//Si[110] and are schematically represented in inset figures of Phi scans.

Transmission electron microscopy (TEM) investigations are performed for both structures for a complete structural characterization. It can be easily observed in both cases that the

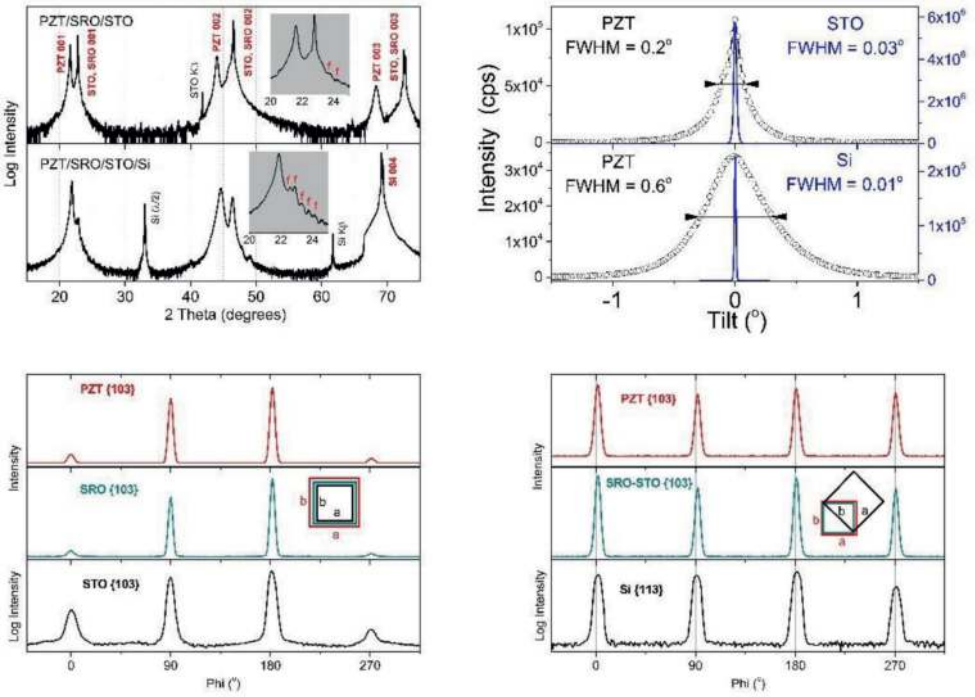

Figure 4. (a) XRD 2Theta-Omega scans (the insets are details around the 001 lines, showing the layer fringes of SRO, or of both SRO and STO thin films, respectively), (b) rocking curves taken at PZT 002, STO 002 and Si 004 lines and (c) phi scans obtained in asymmetric geometry by locating the {103} planes of STO and PZT and the {113} planes of Si (insets, sketches of the in-plane relationships deduced from the phi scans).

SRO and PZT layer thickness is of about 100 and 20 nm, respectively. In the case of the structure deposited on Si substrate, a bright thin layer with thickness of 4 nm is detected at the interface between Si and STO layers, and it is attributed to a native layer of SiO_2. Epitaxial relation between the constituent layers and the orientation relationship between crystallographic planes are revealed from the selected area electron diffraction patterns (SAED). The results obtained for the lattice constant of PZT from SAED images are in accordance with those obtained by XRD, again indicating a more relaxed PZT in the case of Si substrate compared to a more elongated unit cell in the case of PZT deposited on STO substrate. High-resolution TEM (HRTEM) images are acquired in order to observe the quality of the interfaces between the constituent layers. A strain contrast is revealed in the PZT layer in the case of the sample deposited on Si substrate, with a distorted region at the interface with the bottom SRO electrode, region-containing clusters of dislocations (**Figures 5** and **6**).

All the differences observed in the structural quality of the deposited layers and interfaces are having a significant impact on the macroscopic electrical properties of the two structures, as will be presented further on.

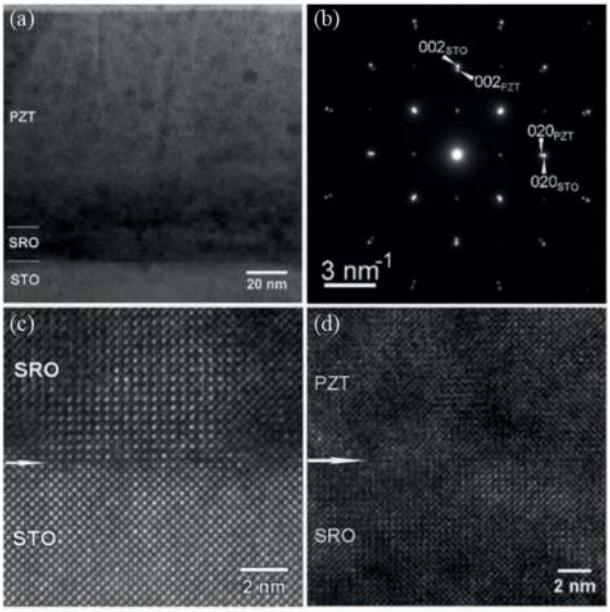

Figure 5. (a) TEM image at low magnification of PZT/SRO/STO heterostructure, (b) SAED pattern corresponding to TEM image (a), (c) HRTEM image of the STO-SRO interface and (d) HRTEM image of the SRO-PZT interface.

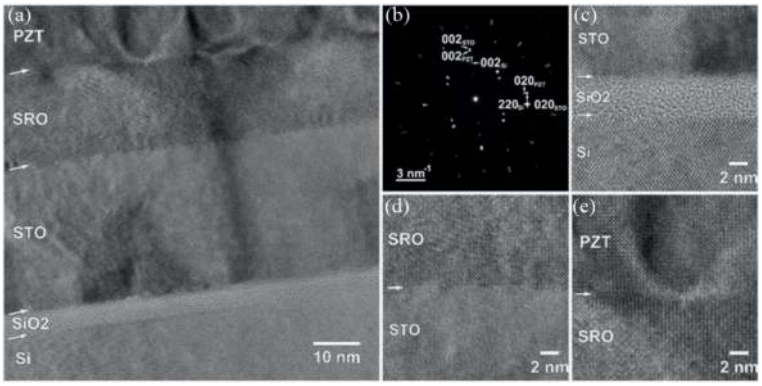

Figure 6. (a) HRTEM image at low magnification of PZT/SRO/STO/Si heterostructures, (b) SAED pattern corresponding to TEM image (a), (c) HRTEM image of the Si-SiO_2-STO interfaces, (d) HRTEM image of the STO-SRO interface and (e) HRTEM image of the SRO-PZT interface.

The presence of the hysteresis loop, describing the change in spontaneous polarization when an external electric field is applied on the ferroelectric capacitor, is the most important property of a ferroelectric material. The defining parameters of the hysteresis loop are saturated polarization (maximum value of polarization), remnant polarization (the value of polarization

at zero applied field) and coercive field (the required electric field to have zero polarization). The classic circuit to record a hysteresis loop is based on the Sawyer-Tower experiment [34]. A similar principle used nowadays, computer controlled equipment, is able to record at the same time both current and charge (polarization) hystereses. The current loop recorded for a ferroelectric capacitor should present the two peaks, one for each polarity of the applied voltage. The peaks are attributed to polarization switching from one direction to the other. The polarization-voltage loop is obtained by integration of the current loop.

The ferroelectric character is checked for the two structures by recording the hysteresis loops, and the obtained results are presented in **Figure 7**. Even if both samples present an epitaxial relation between deposited layers and ferroelectricity is evidenced in both cases by the presence of the switching peaks in the current hysteresis, many relevant properties and values are different. For instance, in the case of the structure deposited on STO substrate, the switching peaks are sharper, and the polarization loop is more rectangular than the case of the structure deposited on Si substrate. In addition, the values of the remnant polarization are different: 26 μC/cm^2 for PZT on Si compared to 48 μC/cm^2 for PZT on STO substrate. The coercive voltage is lower in the case of PZT deposited on Si, 1.3 V compared to 2.5 V for the other structure.

The presence of ferroelectricity is also revealed by the butterfly shape of the capacitance-voltage (C-V) characteristics, which is also related to the switching phenomena by the relation $\varepsilon = \frac{1}{\varepsilon_0}\frac{\partial E}{\partial P}$. The differences between the C-V measurement and the previously described P-V measurement consist in the fact that the former is performed by superimposing a small amplitude AC voltage (to measure the capacitance) over a DC voltage (setting the polarization value), while the latter is performed by applying a variable voltage (sin or triangle waveform) on the sample. Therefore, the C-V measurement is quasi-static, while P-V is dynamic. The C-V characteristics

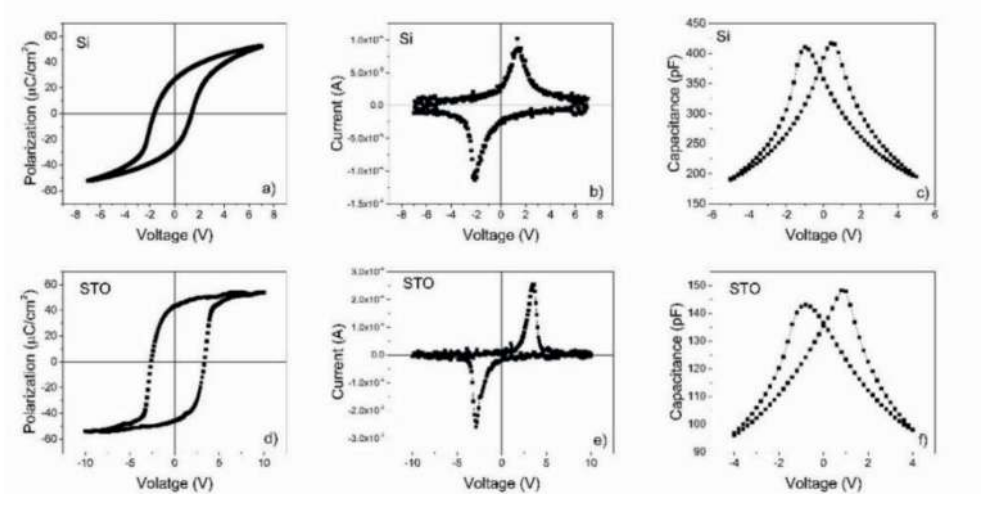

Figure 7. (a and d) Polarization hysteresis loop for PZT deposited on Si substrate and STO substrate, respectively; (b and e) current hysteresis loops; and (c and f) capacitance-voltage characteristics.

are also presented in **Figure 7**. It can be observed that the structures present different shapes of the characteristic and that the values for capacitance and coercive voltages are dependent on the used substrate. In the case of the PZT film deposited on the Si substrate, the value of the dielectric constant at 0 V is 650, much higher than the value of 240 obtained for the PZT film grown on STO substrate. Furthermore, an asymmetry can be observed in the case of PZT/SRO/STO structure. The two capacitance peaks have different values for positive and negative voltage polarities, with a shaper maxima and higher value for positive voltages.

The differences observed between the two structures, and mentioned above, are related to the previously described differences in the structural quality of the ferroelectric films deposited on different substrates. The higher polarization value obtained for the PZT film deposited on the STO substrate is correlated to a higher strain in this case, while the lower value for the film deposited on Si substrate is explained by the increased density of defects in the ferroelectric layer. These defects may suppress the switching of ferroelectric domains, determining a lower polarization value and a slower reversal of polarization, with a larger width of the switching current peaks.

An imprint voltage around 1 V is observed in the hysteresis loop of the structure deposited on the STO substrate, suggesting the presence of an internal electric field oriented towards the top electrode. This internal field cannot be assigned to different work functions of the bottom SRO electrode (4.6–4.9 eV) [35] and top Pt electrode (5.65 eV) [36] as the same electrodes are used for the PZT film deposited on Si substrate. However, the imprint is very much reduced in this case, leading to a more symmetric hysteresis loop, as shown in **Figure 7 (d)**. This is an indication that the internal electric field has a different origin, such as a gradient of the strain distribution or non-homogenous spatial distribution of defects like oxygen vacancies.

Despite these differences, the values of the most important parameters, such as remnant polarization and dielectric constant, belong to the same order of magnitude. This proves that high-quality epitaxial PZT films can be grown by PLD on Si substrates with STO buffer layer, allowing their rapid integration with semiconductor technology. The electric properties can be further tuned by changing the electrode material of the ferroelectric capacitor [37, 38]. The influence of the electrode-ferroelectric interface on the macroscopic electrical properties of epitaxial PZT films has been previously studied [39] for films with tetragonal structure deposited on single-crystal STO substrate, but it was less studied for epitaxial PZT films deposited on Si substrate and with composition near the morphotropic phase boundary [38]. Therefore, different materials were used as top electrodes (Pt, Ir, Ru and an oxide with metallic conduction, SRO) on PZT layer deposited on Si substrate with STO buffer layer.

The hysteresis loops and C-V characteristics obtained at room temperature for all four types of electrodes are presented in **Figure 8**. A first observation is that the shape of the hysteresis loops and the values of the remnant polarizations and coercive fields depend on the material used for the top electrode. For example, in the case of SRO top electrode, the remnant polarization has the highest value around 20 $\mu C/cm^2$ and the highest coercive voltage of 3.7 V. Moreover, both hysteresis and C-V loop are almost symmetric, which is expected due to symmetry of the electrode configuration for this structure (both top and bottom electrodes are SRO). The small shift of the hysteresis, of 0.2 V towards positive voltages, observed in this case can be explained

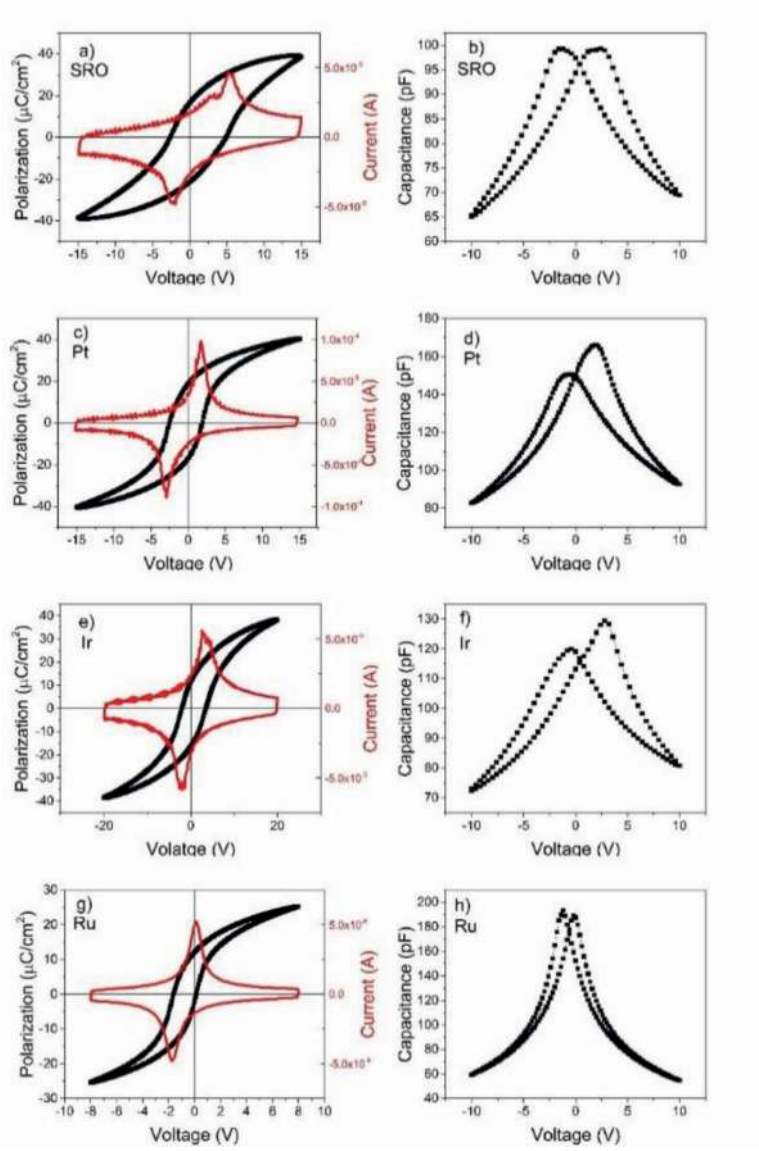

Figure 8. Hysteresis loops and capacitance-voltage characteristics obtained for different top electrodes: (a,b) for SRO, (c,d) for Pt, (e,f) for Ir and (g,h) for Ru, respectively.

by different deposition sequences (PZT deposited on SRO at bottom interface compared to SRO deposited on PZT at top interface), leading to small differences in the electronic properties of the two PZT/SRO interfaces.

The structures with Pt and Ir top electrodes have similar characteristics. This is an expected result considering that Pt and Ir are in the same group of precious metals, with the same structure of the electron shells (same period of the Mendeleev's table). For these two structures, polarization is 12 μC/cm^2, and the coercive voltage is 2.5 V. A shift of the hysteresis loop towards positive voltages is expected in the case of Pt, due to the higher work function for Pt than SRO bottom electrode, but the magnitude of the internal field is much lower than the difference between work functions. In addition, in the case of Ir, there is no shift of the hysteresis loop, even if the difference between work functions is almost 1 eV. These results confirm again that the origin of imprints is related to the different defect distributions at the top and bottom electrode interfaces and not related to the differences between the work functions of the top and bottom electrodes.

The polarization and coercive voltage have much lower values in the case of Ru top electrode—8 μC/cm^2 and 1.2 V, respectively—with an imprint of 0.6 V towards negative voltages. The significant differences obtained in the case of Ru top electrode can be assigned to a Ru oxidation, forming RuO_2, which also has a high conductivity. This process leads to an increased density of oxygen vacancy (which acts as a donor-type defect) at the top interface and, in consequence, to an electric field oriented towards the bottom contact.

The dielectric constant obtained from C-V measurements at maximum applied voltage, where contribution from polarization switching is reduced, is dependent on the material used as top electrode: 392, 523, 443 and 309 for SRO, Pt, Ir and Ru, respectively. One can observe from **Figure 8** that the value of measured capacitance is dependent on the value of the applied voltage. The explanation for this behaviour is that the ferroelectric-electrode interface behaves like a Schottky contact, with an associated Schottky capacitance dependent on interface properties as in the following equation: $C = \sqrt{\frac{q\,\varepsilon_0\,\varepsilon_{st}\,N_{\text{eff}}}{2(V+V_{bi})}}$ [40]. Therefore, the values of N_{eff} and V_{bi} can change when the material for the top electrode is changed, affecting in this manner the capacitance of the entire metal-ferroelectric-metal structure and leading to different capacitance values for negative and positive voltages as observed in the C-V characteristics presented in **Figure 8**.

5. Ferroelectric multilayered thin films: structural and electrical properties

One way to obtain new electrical properties/new phenomena, of interest for new applications, is to deposit multilayered structures by combining ferroelectric thin films with thin films from materials having different properties, for example, ferroelectric/paraelectric, ferroelectric/dielectric and ferroelectric/ferromagnetic, or by introducing composition gradients. Examples of new phenomena experimentally evidenced in multilayered heterostructures are negative capacitance in ferroelectric superlattices, enhancement of the electro-resistance or multiple ferroelectric states. One of the most known categories of multilayered structures is the one of artificial multiferroics, obtained by combining ferroelectric thin films (PZT, $BaTiO_3$-(BTO)) with thin films having magnetic properties ($CoFe_2O_4$-CFO, La_xSr_{1-x} MnO_3-LSMO). Besides at

least two order parameters (ferroelectric polarization and magnetization), these materials also can present magneto-electric coupling mediated by interfacial strain or charge, making them very suitable for future applications and devices.

The electrical and ferroelectric characteristics of multiferroic heterostructures will be presented in this section. The structures were obtained by combining PZT or BTO ferroelectric thin films with CFO layers. The first part of the study consists in analysing the influence of the PZT (20/80)-CFO or BTO-CFO interfaces on the structural, ferroelectric and dielectric properties of the multilayer. Two different configurations, symmetrical (PZT-CFO-PZT or BTO-CFO-BTO) and asymmetrical (PZT-CFO or BTO-CFO), have been selected and deposited on (100) STO single crystal with SRO bottom electrode [41].

The XRD 2θ−ω scans reveal pseudocubic structures of the deposited layers for all cases of symmetric and asymmetric structures and for both ferroelectric layers: the full scan from 10 to 110° presents only 00l peaks for constituent layers: SRO, PZT or BTO and CFO. To prove the epitaxial relation between the deposited layers, azimuth phi scan is performed on {103} skew planes for STO, SRO and PZT and on {115} planes of CFO. The results are shown in **Figure 9** for PZT-based structures which mention that the same results are obtained for BTO-based structures. These results indicate a cube-on-cube epitaxial relation for all four structures, and the in-plane orientation is CFO[100]||PZT[100]||SRO[100]||STO[100].

Figures 10 and **11** present TEM images obtained for multilayered structures. The TEM images at low magnifications reveal the constituent layers as well as their thickness. It can be noticed that the CFO layer has a pyramidal growth with a roughness surface, determined by a Volmer-Weber growth mechanisms determined by the lattice mismatch between PZT and CFO. The first layer of ferroelectric materials (PZT or BTO) is of high quality, as is it expected due to small lattice mismatch between ferroelectric layers and SRO bottom electrode and substrate. The second layer of PZT or BTO in symmetric structures presents an increased density of defects induced by the CFO layers, although the hetero-epitaxy is preserved.

In the experimental study of the multilayered structures, it is very important to decide if their electrical properties are a simple superposition of the bulk properties of the constituent materials or are a result of interface phenomena. For example, when a ferroelectric layer is combined with a paraelectric layer, two competing phenomena are determined by the presence of the interface:

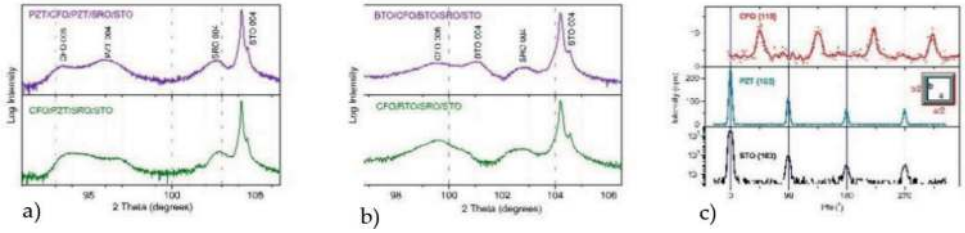

Figure 9. (a) XRD 2θ−ω scans zoomed near STO 004 for PZT-based multilayers structures, (b) XRD 2θ−ω scans zoomed near STO 004 for BTO-based multilayers structures and (c) Phi scans obtained in asymmetric geometry by location the {103} planes of STO and PZT and the {115} planes of CFO.

http://dx.doi.org/10.5772/intechopen.70133

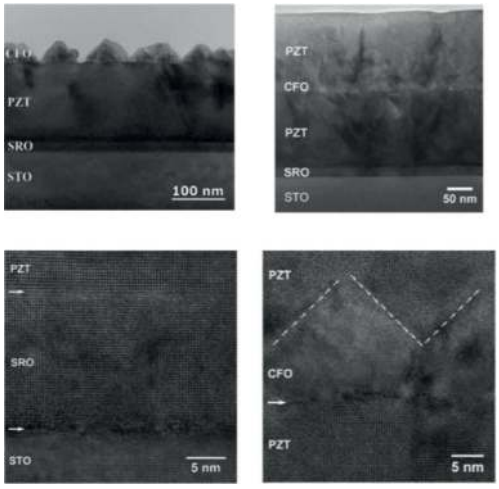

Figure 10. TEM image at low magnification of PZT-CFO and PZT-CFO-PZT heterostructure (first line) and HRTEM images of the STO-SRO, SRO-PZT and PZT-CFO-PZT interfaces (second line).

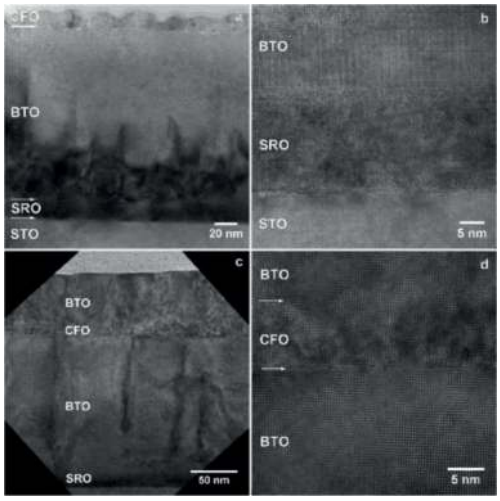

Figure 11. (a)TEM image at low magnification of BTO-CFO heterostructure, (b) HRTEM images of the STO-SRO and SRO-BTO interfaces, (c) TEM image at low magnification of BTO-CFO-BTO heterostructure and (d) HRTEM images of the BTO-CFO-BTO interfaces.

strain fields or strain gradients coming from lattice mismatch between the layers and the associated lattice relaxation mechanisms to reduce the total free energy and depolarization fields with origin in the discontinuity of the polarization charges which will determine different ways of response of the ferroelectric layer such as formation of polydomain structure or transition to a paraelectric state.

The following results show how different electrostatic boundary conditions modify ferroelectric and dielectric properties of multilayered structures. Typical hysteresis loops obtained for epitaxial PZT 20/80 and BTO layers grown on STO substrate with SRO top and bottom electrodes are presented in **Figure 12 (a, d)**. The PZT20/80-based capacitor presents a rectangular shape of the polarization loop, with two sharp current peaks associated to polarization switching from one direction to the other. The remnant and saturated polarization have similar values, around 85 μC/cm^2,, and the coercive field is around 100 kV/cm^2. For the BTO-based capacitor, the remnant polarization is around 15 μC/cm^2, the saturated polarization around 25 μC/cm^2 and the coercive field around 50 kV/cm^2. The polarization hysteresis loop is elongated, and the switching current peaks are broader compared to the PZT case. Those are typical characteristics for these two ferroelectric materials and are further used as references to be compared with the ferroelectric hysteresis loops obtained for asymmetric and symmetric multilayered structures mentioned above.

In what concerns the asymmetric structures, as PZT-CFO or BTO-CFO, the modifications of the hysteresis characteristics are similar for both cases, meaning decrease of the remnant polarization and increase of the coercive field, increase in the width of the switching current peaks and increase of the polarization back switching. These changes are due to imperfect screening of polarization charges at the top interfaces, due to the presence of less conductive CFO layer compared with metallic SRO electrodes. The high depolarization field existing in the system is compensated on the expense of polarization value, which decreases due to the electrostatic coupling between the component layers. Another interesting observation is that, even if the structures are totally asymmetric, with completely different electrostatic boundary conditions at the top and bottom interfaces of the

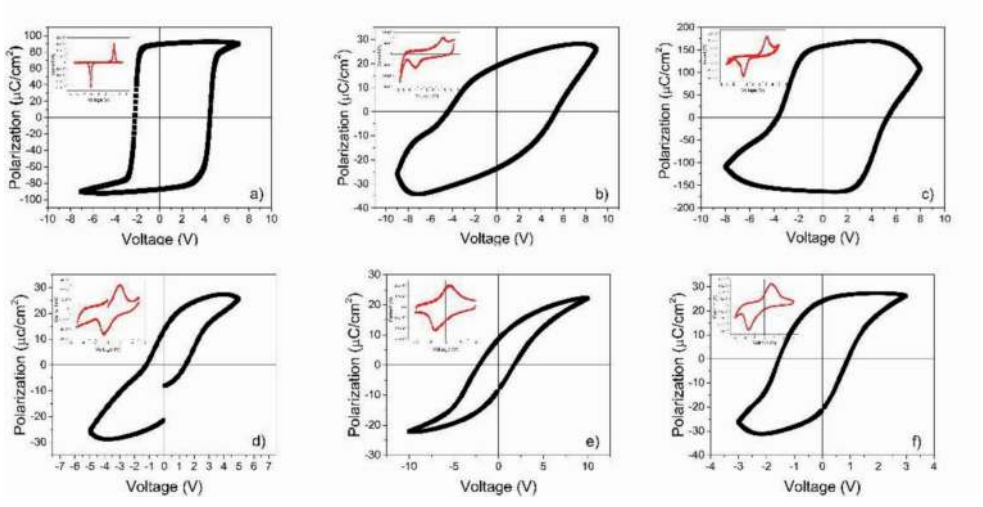

Figure 12. Hysteresis loop for (a) PZT20/80-based capacitor, (b) PZT-CFO asymmetric structure, (c) PZT-CFO-PZT symmetric structure, (d) BTO-based capacitor, (e) BTO-CFO asymmetric structure and (f) BTO-CFO-BTO symmetric structure.

ferroelectric layers, the hysteresis characteristics are approximately symmetric: similar coercive voltages and polarization values for both voltage polarities, with similar amplitude of the switching currents.

The ferroelectric characteristics of symmetric PZT-CFO-PZT and BTO-CFO-BTO structures become similar with the ones of simple metal-ferroelectric-metal structures, with similar values for the polarization and coercive field. The presence of the CFO layer between the ferroelectric films induces a higher leakage current in the case of PZT-based multilayered structure. In the case of BTO-based structure, the effect is opposite, the presence of the CFO layer leading to a lower leakage current and lower back-switching effects, determining in this way a more rectangular shape of the polarization hysteresis loop.

The capacitance-voltage measurements performed at 100 kHz frequency, for the two multilayered structures based on PZT, are depicted in **Figure 13**. The ferroelectric behaviour is also confirmed, for both types of structures, by the butterfly shape of the characteristics. In the case of the asymmetric structure, the capacitance is much lower than in the case of the symmetric structure even if the thickness is lower. Furthermore, the tunability is much lower; the variation of the capacitance value between the peak and the maximum applied voltage is 6 pF, compared to 20 pF in the case of the symmetric structure. In addition, the asymmetry between the values of the capacitance maxima, in the case of the asymmetric structure, can be explained by the presence of asymmetric electrode interfaces, leading to different values of the associated capacitances (different interface properties). The dielectric behaviour is further examined by measuring the dependence on frequency of the capacitance and dielectric losses for the two types of the structures. The results are compared with those obtained on metal-ferroelectric-metal capacitors and on metal-CFO-metal structures. As regards the SRO-PZT-SRO structure, the dielectric behaviour is typical for a ferroelectric/isolator material: there is a small decrease of the capacitance with increasing the frequency, with low values of the dielectric losses. Also, the results obtained on SRO-CFO-SRO structure, presented in **Figure 14 (c–d)** are specific for ferrite-based capacitors [42]:

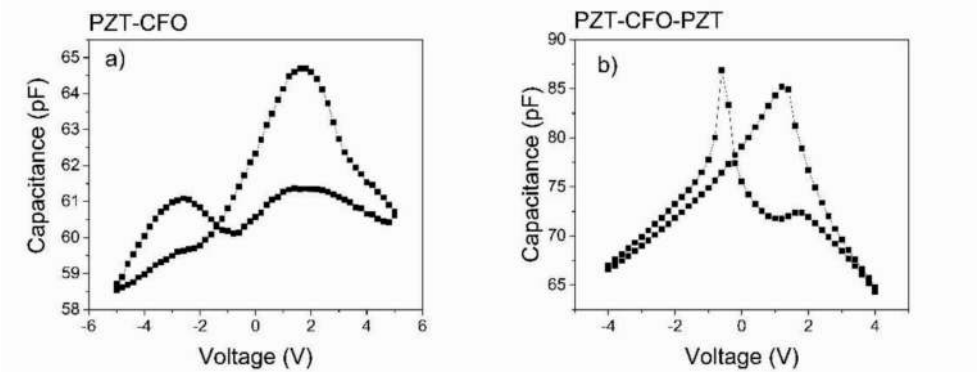

Figure 13. Capacitance voltage characteristics for PZT-based multilayered structures for (a) asymmetric configuration and (b) symmetric configuration.

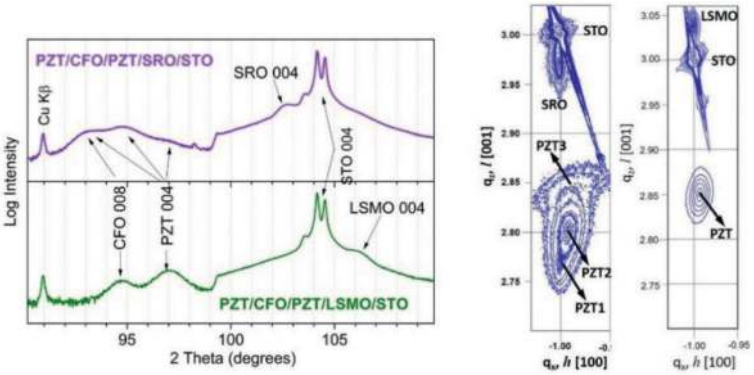

Figure 14. (a) XRD diagrams zoomed near the 004 line of STO and (b) RSM images for PZT-CFO-PZT deposited on SRO bottom electrode (left) and of PZT-CFO-PZT deposited on LSMO bottom electrode (right).

the values of the capacitance present a steplike decrease with frequency, with one order of magnitude difference between low and high frequencies; dielectric losses present a fast decreasing up to 1 kHz, followed by a peak in the frequency range where the capacitance decreases.

The dielectric behaviour for the two types of multilayered structures is different, compared to the behaviour of the single-phase PZT or CFO-based capacitors, and is strongly dependent on the symmetry of the structure. Even if the multilayered structures display steplike decrease of the capacitance with the increase of frequency and peaks in dielectric losses, the values for capacitance and dielectric losses are lower than the case of the simple CFO capacitors. The dependence of the capacitance and dielectric losses on frequency for multilayered structures are determined especially by an additional interface polarization/charge, due to the presence of interfaces between layers of materials with different permittivity and resistivity values. At high frequencies, the value of the capacitance for multilayered structures is closer to that estimated from the serial connection of the capacitors associated to component layers (PZT or CFO). For lower frequencies, the capacitance value is significantly dependent on the number of interfaces, increasing as the number of interfaces in the structure increases. In addition, the position and magnitude of the relaxation peak are strongly related to the configurations of the multilayer structure. Further results will show how different strains and strain gradients influence the ferroelectric and dielectric properties. As an example, we consider two symmetric structures of PZT/CFO/PZT, with thinner PZT layer (50 nm) than previous examples, deposited on two different bottom electrodes SRO and LSMO.

The results of XRD investigations performed on these two symmetric structures, deposited on two different bottom electrodes, are presented in **Figure 14 (a)** for $2\theta-\omega$ around 004 line of PZT and in **Figure 14 (b)** for reciprocal space mapping (RSM). The structure deposited on LSMO electrode presents only a peak for PZT in XRD pattern, corresponding to a bulk out of plane lattice parameter, and only one node in RSM map is attributed to a fully relaxed PZT. The

structure deposited on SRO bottom electrode presents different characteristics: evident splitting of the PZT lines, associated with two nodes in RSM map, having different in-plane and out-of-plane lattice parameters. These values are associated to the two different PZT layers: one

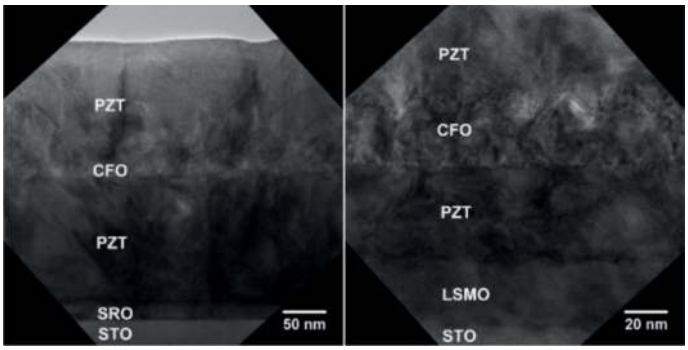

Figure 15. TEM image at low magnification of PZT-CFO-PZT deposited on SRO bottom electrode (left) and of PZT-CFO-PZT deposited on LSMO bottom electrode (right).

fully strained, with in-plane parameter close to STO lattice constant (most probably bottom PZT layer), and one almost fully relaxed, with similar parameters as for the PZT film in structure deposited on LSMO electrode (**Figure 15**).

The ferroelectric behaviour, for both structures, is comparatively presented in **Figure 16** through polarization hysteresis loops and capacitance-voltage characteristics. Both structures present rectangular hysteresis loops and well-evidenced butterfly shape of C-V characteristics. However, a series of differences are easily observed:

- Different values of remnant polarization (90 μC/cm^2 for structure with SRO bottom electrode and 60 μC/cm^2 for structure with LSMO bottom electrode)
- Much higher shift of the hysteresis loop towards positive voltages for the structure deposited on SRO

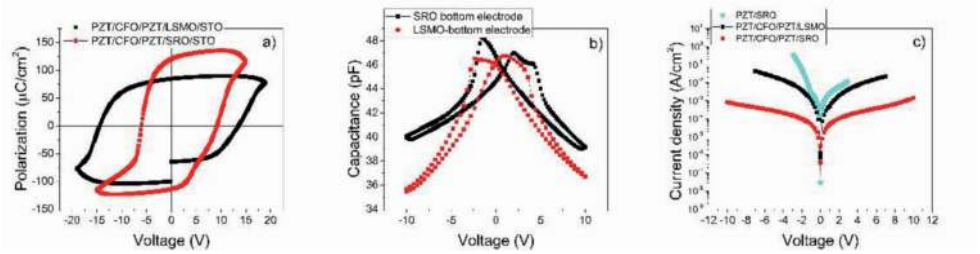

Figure 16. (a) The polarization hysteresis loops; (b) capacitance-voltage characteristics for PZT-CFO-PZT symmetric structure deposited on SRO bottom electrode and LSMO bottom electrode and (c) the dependence of current density on voltage for the two studied structures and compared with a simple thin layer of PZT-based capacitor.

- Higher tunability in the case of LSMO bottom electrode
- A small asymmetry between capacitance maxima in the case of SRO bottom electrode

These differences could be correlated with different structural characteristics determined by XRD and TEM investigations. A totally relaxed structure in the case of the LSMO bottom electrode implies a lower tetragonality and explains lower polarization values. The structural defects, observed in TEM imagines for both PZT layers of this structure, could act as polarization domain pinning centres which determines a slower reversal of polarization from one direction towards the other. The structure deposited on SRO presents two PZT layers with different structural properties. As a consequence, we assume that there is a strain gradient that could be correlated with the existence of an internal electric field pointing towards the top interface that explains the shift observed in the P-V loop of this structure.

A less discussed topic in this chapter, but very important for the operation of ferroelectric devices, is the leakage current. A higher leakage current is detrimental for long-term operation of ferroelectric-based devices. Thus, a significant research effort is dedicated to the identification of the conduction mechanisms, which control the leakage current in ferroelectric thin films and to find a solution to decrease the value of the leakage current. The dependence of the leakage current on voltage (I-V characteristics) is presented in **Figure 17 (c)** for the cases of the two PZT-CFO-PZT structures deposited in SRO and LSMO electrodes. The results are compared with those obtained for a simple PZT capacitor with similar thickness. It is clear that, even if these structures operate at higher voltages, the leakage current is much lower than for a simple PZT layer, the differences being around two orders of magnitude for the structure deposited on SRO.

It was shown in the previous section that the number of interfaces in this multilayered heterostructures determines the dielectric behaviour. Further, **Figure 17** presents the results of the measurements regarding the dependence of the capacitance and dielectric losses, on frequency and temperature, for these two symmetrical structures, with different strain conditions and structural quality of the ferroelectric layers. The values of capacitance and dielectric losses at temperatures below 250 K are similar to those obtained for single-phase PZT capacitor presented in **Figure 18**. This behaviour is modified towards a Maxwell-Wagner mechanism with an increase in temperature, specific for multilayered structures with interfaces between materials with different electric properties. The transition between low-temperature and high-temperature dielectric behaviour can be correlated with a strong variation of the resistivity of the CFO layer with temperature as is exemplified in **Figure 17 (f)**. Therefore, the difference in resistivity between PZT and CFO layers will increase with temperature, favouring in this way Maxwell-Wagner polarization mechanism. The capacitance at lower frequencies and the relaxation marked by the peak in dielectric losses are strongly dependent on the structure and on the temperature. It can be observed that for the structure deposited on LSMO electrode, the values of the capacitance at lower frequencies are higher, and the frequency where the maximum in dielectric losses occurs is higher than for the structure deposited on SRO, at the same temperature.

http://dx.doi.org/10.5772/intechopen.70133

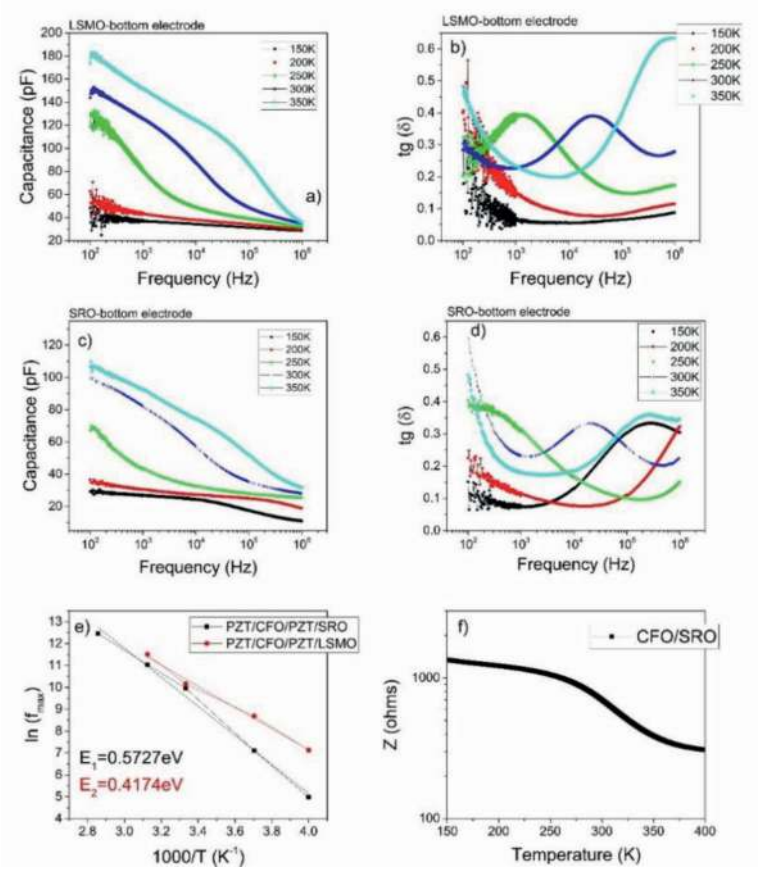

Figure 17. (a and b) The dependence of capacitance and dielectric losses, respectively, on frequency and for different temperatures for LSMO bottom electrode case; (c and d) the dependence of capacitance and dielectric losses, respectively, on frequency and for different temperatures for SRO bottom electrode case; (e) the Arrhenius plot of the maximum dielectric losses frequencies and (f) the variation of impedance of a thin layer CFO-based capacitor on temperature.

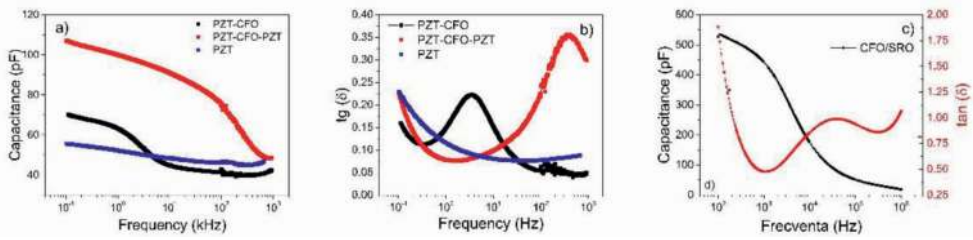

Figure 18. (a) The dependence of capacitance on frequency, (b) the dependence of the dielectric loses on frequency comparatively presented for PZT-based structures and (c) the dependence of capacitance and dielectric losses on frequency for a thin layer of CFO-based capacitor.

6. Conclusions

This chapter presents the electrical properties of epitaxial ferroelectric thin films and multilayers. A short description of the deposition/growing steps used to obtain high-quality epitaxial ferroelectric structures, with sharp interfaces, is presented at the beginning. The main experimental results show how ferroelectric and dielectric properties depend on the structural quality of the ferroelectric layer and on the electrostatic boundary conditions.

Acknowledgements

The authors acknowledge the financial support of the Romanian Ministry of Education-Executive Unit for Funding High Education, Research, Development and Innovation (MEN-UEFISCDI) through the Nucleus Program PN16-4801; the Idea-Complex Research Grant PN-II-ID-PCCE-2011-2-0006 (Contract No. 3/2012); the IFA-CEA (Contract No. C503/2016); and the CNCS-UEFISCDI Project of PN-II-PT-PCCA-2013-4-0470 (Contract No. 238/2014).

Author details

Andra Georgia Boni*, Cristina Florentina Chirila, Raluca Negrea, Corneliu Ghica, Iuliana Pasuk, Ioana Pintilie and Lucian Pintilie

*Address all correspondence to: andra.boni@infim.ro

National Institute of Materials Physics, Bucharest-Magurele, Romania

References

[1] Scott JF. Applications of modern ferroelectrics. Science. 2007 Feb 16;**315**(5814):954-959

[2] Lallart M, editor. Ferroelectrics - Applications [Internet]. InTech; 2011. Available from: http://www.intechopen.com/books/ferroelectrics-applications

[3] Okuyama M, Ishibashi Y, editors. Ferroelectric Thin Films [Internet]. Berlin, Heidelberg: Springer Berlin Heidelberg; 2005. (Ascheron CE, Kölsch HJ, Skolaut W, editors. Topics in Applied Physics; vol. 98). Available from: http://link.springer.com/10.1007/b99517

[4] Scott JF. Ferroelectric Memories [Internet]. Berlin, Heidelberg: Springer Berlin Heidelberg; 2000. (Itoh K, Sakurai T, editors. Springer Series in Advanced Microelectronics; vol. 3). Available from: http://link.springer.com/10.1007/978-3-662-04307-3

[5] Eerenstein W, Mathur ND, Scott JF. Multiferroic and magnetoelectric materials. Nature. 2006;**442**:759-765. doi: 10.1038/nature05023. Available from: http://www.nature.com/nature/journal/v442/n7104/full/nature05023.html

[6] Khomskii D. Classifying multiferroics: Mechanisms and effects. Physics. 2009 Mar 9;**2**:20

[7] Scott JF. Data storage: Multiferroic memories. Nature Materials. 2007 Apr;**6**(4):256-257

[8] Loidl A, von Loehneysen H, Kalvius GM. Multiferroics. Journal of Physics: Condensed Matter. 2008 Oct 7;**20**(43):430301

[9] Martin LW, Crane SP, Chu Y-H, Holcomb MB, Gajek M, Huijben M, et al. Multiferroics and magnetoelectrics: Thin films and nanostructures. Jounal of Physics: Condensed Matter. 2008 Oct 29;**20**(43):434220

[10] Matthews J editor. Epitaxial Growth. USA. Elsevier; 2012. p. 401

[11] Pintilie L, Teodorescu CM, Ghica C, Hrib LM, Chirila C, Trupina L, et al. Interfaces in epitaxial structures based on oxide ferroelectrics. In: Composite, Ceramic, Quasi-Crystals, Nanomaterials, High Temperature Protection Coatings. Quebec/Wilmington, Canada/USA: FLOGEN; 2014

[12] Nguyen MD, Dekkers M, Houwman E, Steenwelle R, Wan X, Roelofs A, et al. Misfit strain dependence of ferroelectric and piezoelectric properties of clamped (001) epitaxial Pb(Zr0.52,Ti0.48)O3 thin films. Applied Physics Letters. 2011 Dec 19;**99**(25):252904

[13] Pertsev NA, Kukhar VG, Kohlstedt H, Waser R. Phase diagrams and physical properties of single-domain epitaxial Pb({Zr_{1-x},Ti_x}) O_3 thin films. Physical Review B. 2003 Feb 28;**67**(5):054107

[14] Jang HW, Kumar A, Denev S, Biegalski MD, Maksymovych P, Bark CW, et al. Ferroelectricity in strain-free $SrTiO_3$ thin films. Physical Review Letters. 2010 May 13;**104**(19):197601

[15] He F, Wells BO, Shapiro SM. Strain phase diagram and domain orientation in $SrTiO_3$ thin films. Physical Review Letters. 2005 May 2;**94**(17):176101

[16] Zubko P, Catalan G, Buckley A, Welche PRL, Scott JF. Strain-gradient-induced polarization in $SrTiO_3$ single crystals. Physical Review Letters. 2007 Oct 19;**99**(16):167601

[17] Schlom DG, Chen L-Q, Eom C-B, Rabe KM, Streiffer SK, Triscone J-M. Strain tuning of ferroelectric thin films*. Annual Review of Materials Research. 2007;**37**(1):589-626

[18] Polakowski P, Müller J. Ferroelectricity in un-doped hafnium oxide. Applied Physics Letters. 2015 Jun 8;**106**(23):232905

[19] Bousquet E, Dawber M, Stucki N, Lichtensteiger C, Hermet P, Gariglio S, et al. Improper ferroelectricity in perovskite oxide artificial superlattices. Nature. 2008 Apr 10;**452**(7188):732-736

[20] Jeon BC, Lee D, Lee MH, Yang SM, Chae SC, Song TK, et al. Flexoelectric effect in the reversal of self-polarization and associated changes in the electronic functional properties of BiFeO3 thin films. Advanced Materials. 2013 Oct 1;**25**(39):5643-5649

[21] Lee D, Jeon BC, Yoon A, Shin YJ, Lee MH, Song TK, et al. Flexoelectric control of defect formation in ferroelectric epitaxial thin films. Advanced Materials. 2014 Aug 1;**26**(29):5005-5011

[22] Zhang J, Xu R, Damodaran AR, Chen Z-H, Martin LW. Understanding order in compositionally graded ferroelectrics: Flexoelectricity, gradient, and depolarization field effects. Physical Review B. 2014 Jun 13;**89**(22):224101

[23] Crystal Growth Beginners - AbeBooks [Internet]. Available from: https://www.abebooks.com/book-search/title/crystal-growth-beginners/

[24] Jaffe B, Cook WR, Jaffe H. In: Cook BJR, Jaffe H, editors. Piezoelectric Ceramics [Internet]. Academic Press; 1971. p. v. Available from: http://www.sciencedirect.com/science/article/pii/B9780123795502500041

[25] Kim DM, Eom CB, Nagarajan V, Ouyang J, Ramesh R, Vaithyanathan V, et al. Thickness dependence of structural and piezoelectric properties of epitaxial $Pb(Zr_{0.52,}Ti_{0.48})O_3$ films on Si and $SrTiO_3$ substrates. Applied Physics Letters. 2006 Apr 3;**88**(14):142904

[26] Uchino Kenji. Piezoelectric Actuators and Ultrasonic Motors [Internet]. Springer; 1997. Available from: http://www.springer.com/us/book/9780792398110

[27] Noheda B, Gonzalo JA, Cross LE, Guo R, Park S-E, Cox DE, et al. Tetragonal-to-monoclinic phase transition in a ferroelectric perovskite: The structure of $PbZr_{0.52}Ti_{0.48}O_3$. Physical Review B. 2000 Apr 1;**61**(13):8687-8695

[28] Zhu Y, Yan P, Yi T, Cao L, Li L. Interface diffusion and chemical reaction on the interface of a PZT film/Si(III) sample during annealing treatment in N_2 and vacuum. Surface and Interface Analysis. 1999 Nov 1;**27**(11):972-980

[29] Lin A, Hong X, Wood V, Verevkin AA, Ahn CH, McKee RA, et al. Epitaxial growth of $Pb(Zr_{0.2}Ti_{0.8})O_3$ on Si and its nanoscale piezoelectric properties. Applied Physics Letters. 2001 Apr 2;**78**(14):2034-2036

[30] Basit NA, Kim HK, Blachere J. Growth of highly oriented $Pb(Zr, Ti)O_3$ films on MgO-buffered oxidized Si substrates and its application to ferroelectric nonvolatile memory field-effect transistors. Applied Physics Letters. 1998 Dec 28;**73**(26):3941-3943

[31] Wang Y, Ganpule C, Liu BT, Li H, Mori K, Hill B, et al. Epitaxial ferroelectric $Pb(Zr, Ti)O_3$ thin films on Si using $SrTiO_3$ template layers. Applied Physics Letters. 2002 Jan 7;**80**(1):97-99

[32] Wen-Chieh Shih, Pi-Chun Juan, and Joseph Ya-min Lee. Fabrication and characterization of metal-ferroelectric $(PbZr_{0.53}Ti_{0.47})O_3$-Insulator (Y_2O_3)-ssemiconductor field effect transistors for nonvolatile memory applications. Journal of Applied Physics. 2008 May 1;**103**(9):094110

[33] Chirila C, Boni AG, Pasuk I, Negrea R, Trupina L, Rhun GL, et al. Comparison between the ferroelectric/electric properties of the $PbZr_{0.52}Ti_{0.48}O_3$ films grown on Si (100) and on STO (100) substrates. Journal of Material Science. 2015 Mar 14;**50**(11):3883-3894

[34] Physics of Ferroelectrics [Internet]. Berlin, Heidelberg: Springer Berlin Heidelberg; 2007. (Topics in Applied Physics; vol. 105). Available from: http://link.springer.com/10.1007/978-3-540-34591-6

[35] Hartmann AJ, Neilson M, Lamb RN, Watanabe K, Scott JF. Ruthenium oxide and strontium ruthenate electrodes for ferroelectric thin-films capacitors. Applied Physics A. 2000 Feb;**70**(2):239-242

[36] Schaeffer JK, Fonseca LRC, Samavedam SB, Liang Y, Tobin PJ, White BE. Contributions to the effective work function of platinum on hafnium dioxide. Applied Physics Letters [Internet]. 2004 Sep 6;**85**(10). Available from: http://www.osti.gov/scitech/biblio/20632781

[37] Pintilie L, Alexe M. Metal-ferroelectric-metal heterostructures with Schottky contacts. I. Influence of the ferroelectric properties. Journal of Applied Physics. 2005 Dec 15;**98**(12):124103

[38] Boni AG, Chirila C, Pasuk I, Negrea R, Trupina L, Le Rhun G, et al. Electrode interface controlled electrical properties in epitaxial $Pb(Zr_{0.52}Ti_{0.48})O_3$ films grown on Si substrates with $SrTiO_3$ buffer layer. Thin Solid Films. 2015;**593**:124-130

[39] Pintilie I, Teodorescu CM, Ghica C, Chirila C, Boni AG, Hrib L, et al. Polarization-control of the potential barrier at the electrode interfaces in epitaxial ferroelectric thin films. ACS Applied Material Interfaces. 2014 Feb 26;**6**(4):2929-2939

[40] Sze SM. Physics of Semiconductor Devices [Internet]. 2nd ed. John Wiley & Sons; Available from: https://archive.org/details/PhysicsOfSemiconductorDevices

[41] Chirila C, Ibanescu G, Hrib L, Negrea R, Pasuk I, Kuncser V, et al. Structural, electric and magnetic properties of $Pb(Zr_{0.2}Ti_{0.8})O_3$–$CoFe_2O_4$ heterostructures. Thin Solid Films. 2013 Oct 31;**545**:2-7

[42] Gutiérrez D, Foerster M, Fina I, Fontcuberta J, Fritsch D, Ederer C. Dielectric response of epitaxially strained $CoFe_2O_4$ spinel thin films. Physical Review B. 2012 Sep 10;**86**(12):125309